Computational Analysis of the Fluid-Structure Interaction occurring in a model of Two Vehicles Overtaking Each Other

IOP Conf. Series: Journal of Physics: Conf. Series **1106** (2018) 012009 doi:10.1088/1742-6596/1106/1/012009

Computational Analysis of the Fluid-Structure Interaction occurring in a model of Two Vehicles Overtaking Each Other

Hayder Al-Jelawy[1], Stefan Kaczmarczyk[1], Matthew Cross[2], Rob Lewis[2], Nishant Singh[1], Dhirgham Alkhafaji[3]

[1] Faculty of Arts, Science and Technology, Engineering and Technology Department, The University of Northampton, UK.

[2] TotalSim Ltd. UK.

[3] College of Engineering, The University of Babylon, Iraq.

The corresponding author's e-mail: hayder_sabah56@yahoo.com

Abstract. A computational study has been conducted to investigate the transient aerodynamic forces experienced by two vehicles overtaking each other. Ahmed body model has been used to represent the vehicles. The transient effects during the overtaking scenario have been determined by using a Computational Fluid Dynamics (CFD) model. This has been achieved by developing an open source computational code. The aerodynamic effects have been investigated by emulating this event in a virtual wind tunnel. One of the generic vehicles was set to be stationary, while the other was allowed to be moving at constant speed. The Delayed Detached Eddy simulation (DDES) turbulence approach has been applied in this study based on the finite volume analysis (FVA). The computational results such as fluid forces and moments acting on the vehicle structures have been compared against published experimental results. Encouraging correlations between those results are observed. In the present work, the fluid-structure interaction (FSI) phenomenon has also been studied by developing a flexible body dynamic model. The modal and dynamic responses are determined from FEM analysis by the application of fluid transient loads obtained from the CFD model. This investigation is important to address the issue of stability and performance of the vehicle system. This work provides a significant understanding into the complex aerodynamics of an overtaking process and gives the foundation for further analysis in the area of fluid-structure interactions for more complex geometries and scenarios.

1. Introduction

On one hand, the dynamic response of the vehicle structure has been an active area of research which would affect the vehicle suspension system. This system is an important component which would alleviate the influence of forces excited by the road conditions [1]. On the other hand, the aerodynamic forces and moments are the key role of causing the vibration of any moving vehicle such as a road car, train and a lift car, see [2], [3] and [4].

In their work, [5] were first proposed the Ahmed body which is a generic car model considered as a bluff body in the community of aerodynamics as it has proximity to the ground. Ahmed body has three essential parts, namely a flat top and bottom panels, a rounded front section and the back slant is angled with a vertical back base at the rear. This model is widely studied in literature for better understanding

the flow dynamics in the wake region of the body as well as the fluid forces are experienced in a wide range of configurations [6]. It has been also a reliable experimental database for several of aerodynamic investigations of CFD models [7], [8]. The flow over this type of vehicles is fully three-dimensional flow.

Therefore, the aerodynamic effects can play a significant role on cars vibration which could lead to instability. The objective of this paper is to studying and fully understanding the linear dynamic response which can be the reference of designing a more aerodynamically efficient vehicles. The above CFD common case study can be coupled to the finite element techniques to test the impact of the aerodynamic three forces and moments on the dynamic behaviour of the body. In particular, the overtaking manoeuvre causes additional forces and moments because of the sudden change of the fluid effects.

In the last two decades, an open-source code has been a common tool in academic research [9], [10] and it is attracting the attention of industrial users for multi-physics simulations and adjoined optimization as well [11], [12] and [13]. It has been a research platform and a black-box CFD and structural analysis solver. The CAD model has been generated by using solid modelling commercial software [14]. Another commercial package has been implemented to solve for the finite element analysis. This software is a CAE specific direct modeller which features a robust meshing solution and CAD clean-up workflow. This software provides a direct modelling for FEA to calculate a range of disciplines such as structural deformations, stress and vibrations. It uses matrix methods to process the finite elements which leads to the required results [15].

2. Ahmed Body geometry

The Ahmed body geometry used in [16] and scaled by 7/10 as shown in figure (1).

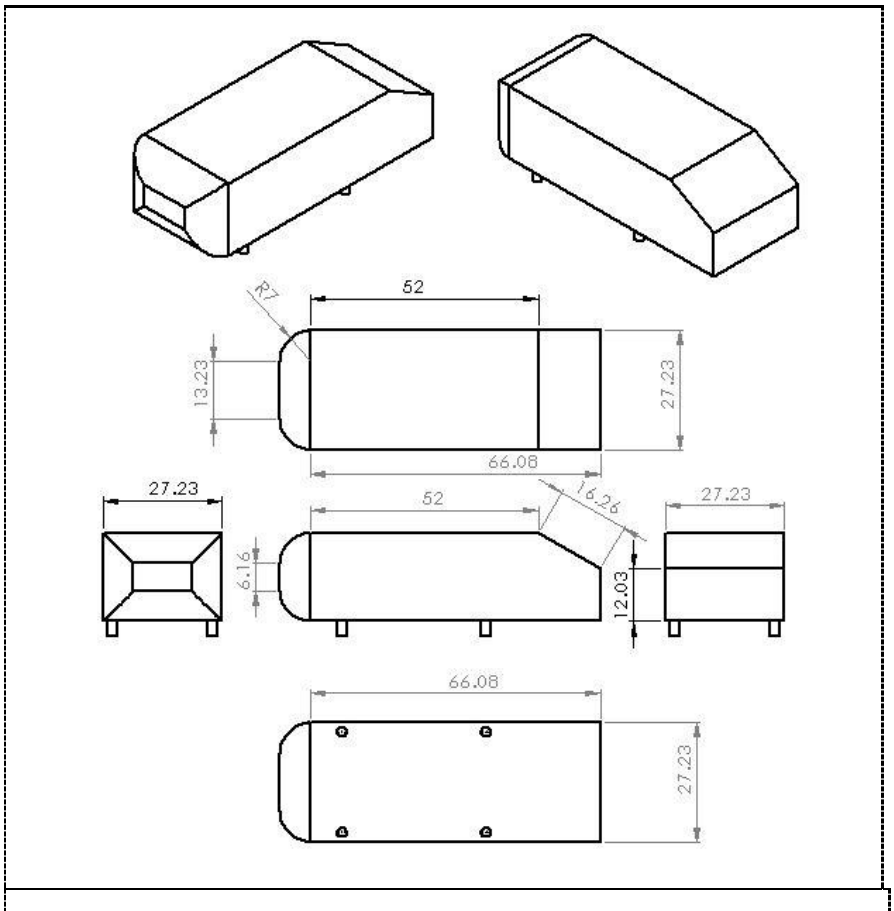

Figure 1. Ahmed bluff body, all dimensions are in cm.

As shown in the figure, the slant angle is 30° and the vehicle dimensions are (73.8, 27.3 and 20.16 cm) as the length, width and height, respectively. The ground clearance is set to be 55 mm. In addition, the Reynolds number based on the vehicle's height is equal to 3.9×10^5 as the velocity is $30.32\ {}^{m}/_{s}$.

3. The wind tunnel

The numerical domain is shown in figure (2). The virtual wind tunnel has been generated by using the BlockMesh dictionary which is available within the open-source software.

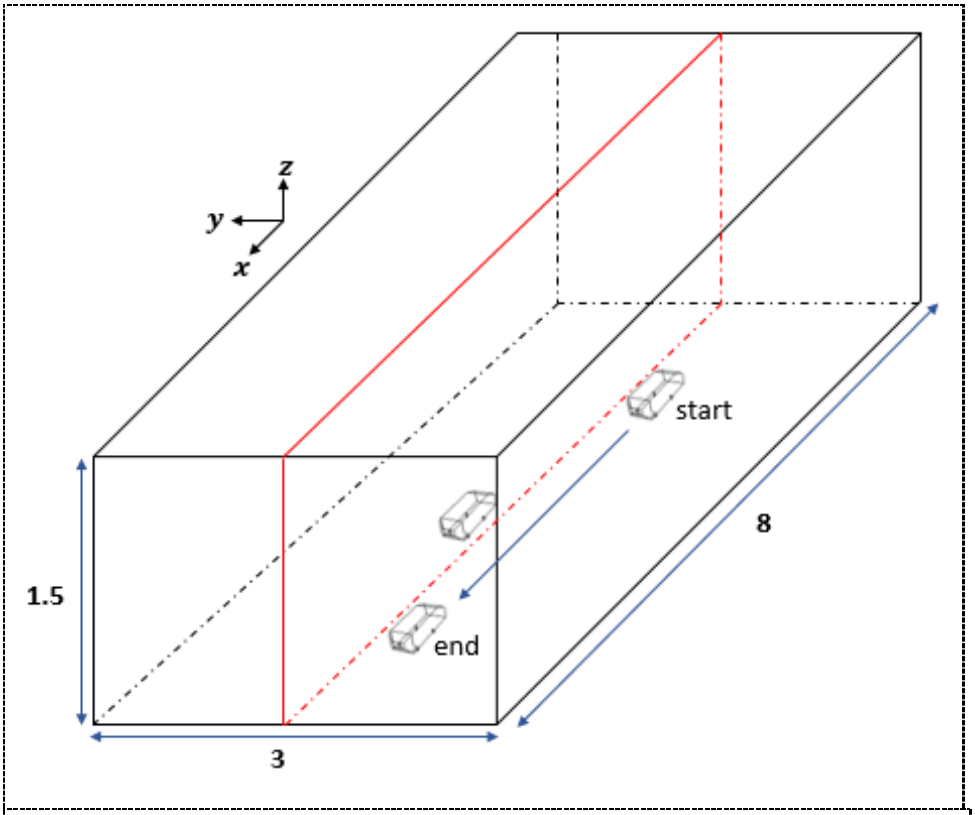

Figure 2. The wind tunnel layout

The length is set to be 8 m in order to have enough time for the simulation progress in terms of the mesh deformation. The uniform velocity was equal to 30.32 m/s at the inlet boundary. The pressure was applied to be static at the outlet boundary. The Ahmed body and the lower wall was set to be No-slip boundary conditions.

4. The fluid flow modelling

The RANS (Reynolds Averaged Navier Stokes equations) has been used to predict the flow behaviour around the vehicles. The conservation of momentum and mass equations are shown below:

$$\frac{\partial(\rho\widetilde{u_\iota})}{\partial x_j} = 0 \tag{1}$$

$$\rho\frac{\partial\widetilde{u_\iota}}{\partial t} + \rho\widetilde{u_\iota}\frac{\partial\widetilde{u_\iota}}{\partial x_j} = -\frac{\partial\tilde{p}}{\partial x_j} + \frac{\partial}{\partial x_j}\left(\rho\nu\frac{\partial\widetilde{u_\iota}}{\partial x_j} - \rho\widetilde{u_\iota' u_j'}\right) \tag{2}$$

where: $\widetilde{u_i}$ $\tilde{p}$ denote the mean velocity and pressure components, respectively. The Reynolds stresses are shown as $\rho\widetilde{u_i'u_j'}$; where: u_i', u_j' refer to the turbulent fluctuation values. Also, ρ denotes the air density and ν is the kinematic viscosity. The parameters also t, u_i denote the time and velocity components in the x_i direction.

In the transient state, the hybrid $\boldsymbol{SST\ k-\omega}$ turbulence model is used to solve the aerodynamic coefficients during an overtaking event of two bluff bodies [17]. The modelled equations for the specific turbulence kinetic energy (k) and the specific dissipation rate (ω) (turbulence frequency) are shown as follows:

$$\frac{\partial(\rho k)}{\partial t}+\frac{\partial\left(\rho k u_j\right)}{\partial x_j}=\widetilde{P_k}-\beta^*\rho\omega k+\frac{\partial}{\partial x_j}\left[\left(\mu+\sigma_k\frac{\rho k}{\omega}\right)\frac{\partial k}{\partial x_j}\right] \tag{3}$$

$$\frac{\partial(\rho\omega)}{\partial t}+\frac{\partial\left(\rho\omega u_j\right)}{\partial x_j}=\alpha\rho S^2-\beta\rho\omega^2+2(1-F1)\sigma_d\frac{\rho}{\omega}\frac{\partial k}{\partial x_j}\frac{\partial\omega}{\partial x_j}+\frac{\partial}{\partial x_j}\left[\left(\mu+\sigma_\omega\frac{\rho k}{\omega}\right)\frac{\partial\omega}{\partial x_j}\right] \tag{4}$$

where: P_k denotes the production limiter; $\beta, \beta^*, \alpha, \sigma_\omega, \sigma_d, \sigma_k$ denote the closure coefficients in the turbulence-rate equation to be 0.075, 0.09, 0.55, 0.5, 0.856 and 0.85, respectively [17]; μ denotes the dynamic viscosity; S denotes the strain rate; $F1$ is the first blending function.

Two blending functions are used in this numerical model to keep the k-ω model active at the region near the wall. Then, it will switch to the k-ε model outside the boundary layer region.

An open source package has been used to solve the system which is applicable for simulating a wide range of CFD applications. It is based on a cell-centred Finite Volume Method (FVM).

The SIMPLE algorithm explained in [18] has been used in the steady state to run a potential solution to initialise the flow. The simulation stability has been approached by running 500 iterations with a limited pressure gradient. The solution has been converged by running another 500 iterations without any limitation of the pressure gradient. The results from the steady state can be used as initial conditions for the transient solution.

Eventually, a transient solver has been set with a new turbulence variables for the Delayed Detached Eddy Simulation (DDES) turbulence model. The DDES model is a combination between both the speed of RANS modelling at the boundary region and the accuracy of Large Eddy Simulation (LES) modelling at the core region and so is called a hybrid solver as published in [19]. The Delayed model uses two blended functions which work very well with the high Reynolds number. Then, the hybrid PIMPLE algorithm which combines the SIMPLE and PISO algorithms which has been used for transient calculations, see [20].

5. The structure modelling

The above system can be considered as a multi-body system (MBS) with various distributed parameters such as discrete and/or continuous components. The multi-body dynamic consists of solid bodies connected to links by joints which can restrict their relative motion. The study of the MBD is to analyse the effects of excitations which can move mechanism systems and it can also be called forward dynamics. In contrast, the inverse dynamics address the necessary excitations which could move a mechanical system. The Ahmed body car suspension system can be shown in figure (3).

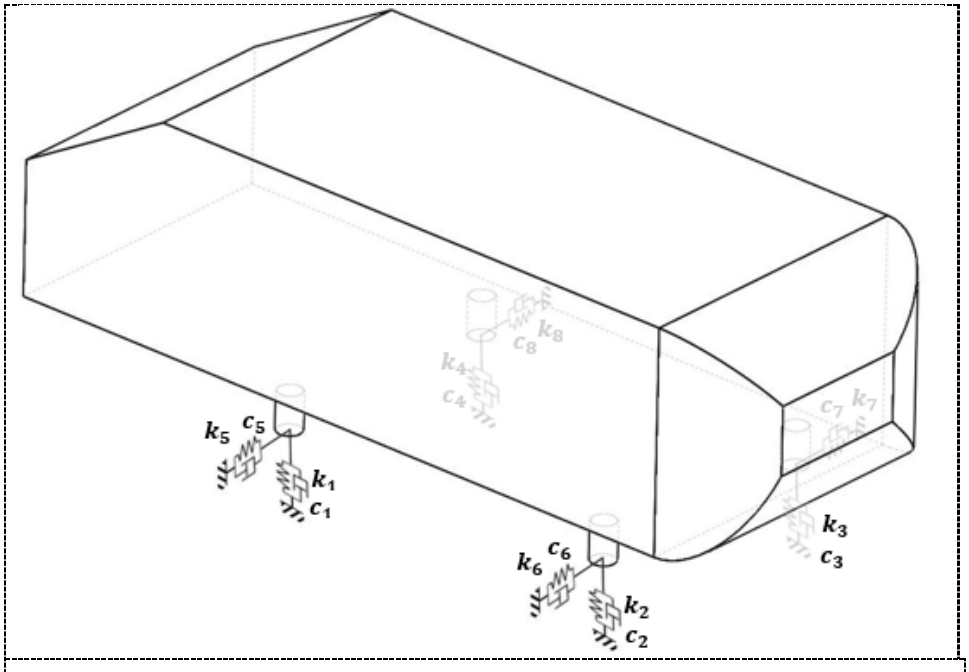

Figure 3. Ahmed body model shows its suspension system

A proper level of accuracy can be achieved and a mathematical and physical description of the mechanism can be constructed. It seems that the FEA analysis is readily applicable to predict the dynamic behaviour of this kind of systems. Ahmed body dynamics due to the fluid forces will be studied in this work, and the simulation tool has been developed to capture specific phenomena or instability.
The fluid-structure interaction is considered to be a one-way coupling method due to the small deformation. This means that only the fluid pressure acting on the body calculated from the fluid solver will be transferred to the structure solver [21].
The impulse conservation equation below has been developed by using the Lagrange's approach [22]. It can be solved by using one of the FEA approaches.

$$[M]\{\ddot{x}(t)\} + [C]\{\dot{x}(t)\} + [K]\{x(t)\} = \{F_i(t)\} \quad (5)$$

where: $[M]$ denotes the mass matrices for the body, $[K]$ and $[C]$ are the system stiffness and damping matrices, $\{\ddot{x}(t)\}, \{\dot{x}(t)\}$ and $\{x(t)\}$ represent the system acceleration and displacement vectors at time t. The fluid forces are denoted by $\{F_i(t)\}$.
The body mass is estimated to be equal to 9.5 kg and the aluminium alloys were used as a body material. The stiffness and damping of each of the springs can be obtained from the following two equations.

$$k_e = 4\pi^2 m f^2 \quad (6)$$

$$c_e = 2\zeta\sqrt{k_e m} \quad (7)$$

where: k_e and c_e denote the effective stiffness and damping coefficients, respectively; m represents the Ahmed body mass; ζ denotes the damping ratio. The natural frequency f has been chosen from one of the natural rigid modes listed in table 1. Therefore, the stiffness and damping coefficients can be equal to 1202.85 $^{N}/_{m}$ and 76.57 $^{(N\ s)}/_{m}$, respectively.

6. CFD mesh generation

Two meshing strategies are available within the OpenFOAM package. BlockMesh utility has been utilised to generate a simple block consists of 81000 cells which are fully structured as a hexahedral mesh. Then, the CAD model has been imported to OpenFOAM from SolidWorks as STL file. It was checked to be as smooth as possible and the correct orientation and position have been accomplished.

Eventually, the snappyHexMesh utility was implemented to generate a high quality hex-dominant mesh. The total mesh volume after using the snappyHexMesh technique was 17,119,330 cells. This mesh has been accomplished in fully parallel execution. The wall layers have been added on both car structures and all boundary conditions to have a better prediction to the flow near wall. The refined mesh near each car surface is shown in figure (4).

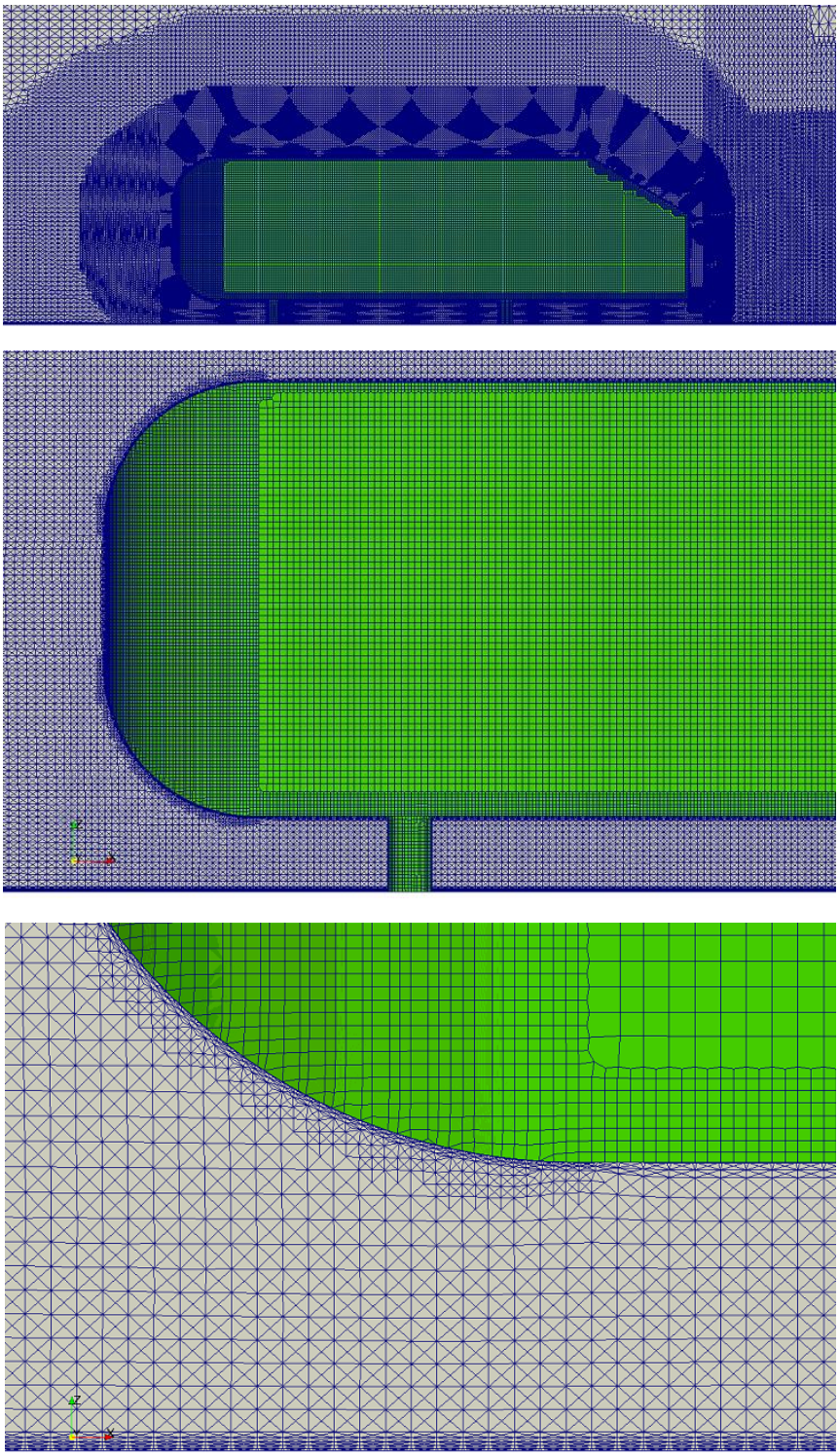

Figure 4. The surface and volume mesh of one car

The cell next to the wall thickness is equal to 0.3 mm and the wall function approach has been implemented which allows the dimensionless wall distance y^+ to be between 30 and 300 as mentioned in [23]. The y^+ average value in this simulation at the log-law region was approximately 75. The y+ is a non-dimensional distance which is used in CFD to describe how coarse of fine the mesh is for a particular fluid flow.

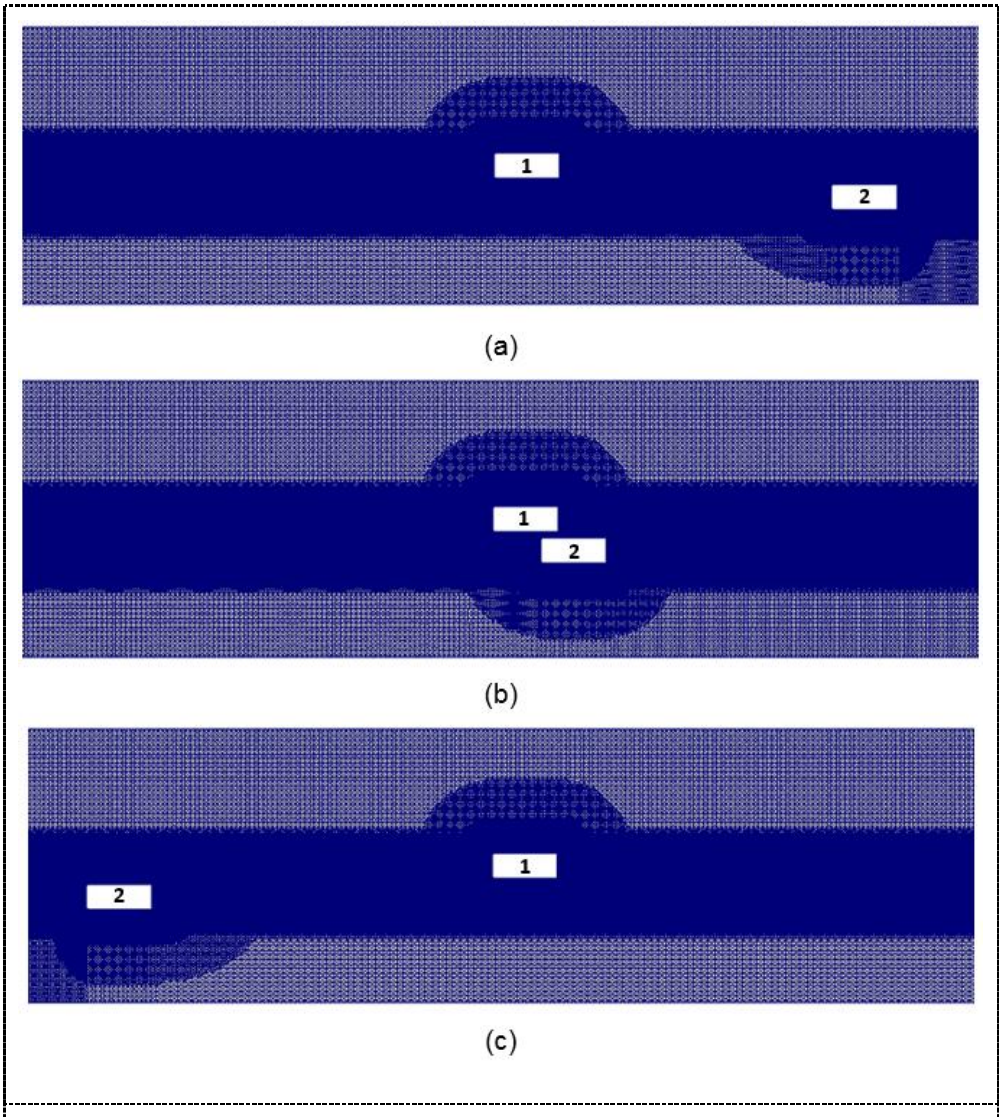

Figure 5. The computational mesh deformation for the overtaking manoeuvre. (a) Start, (b) at the overtaking event, (c) end.

The dynamic mesh technique was used to achieve the rectilinear displacement of the body which allows to control the mesh deformation and sliding. The movement of the mesh is illustrated in figure (5) at three different times of the scenario. Two subdomains were used, the stationary (overtaken) car 1 is located in the top subdomain, while, the moving (overtaking) car 2 is located in the bottom subdomain as shown in the figure above. The scenario was successfully used for two trains pass each other as illustrated in [24].

7. The FEA dynamic scenario

Figure (6) shows the body mesh as well as the suspension system at the pre-possessing stage for FEA study. The fluid forces/moments calculated during the CFD simulation have been applied through the centre of pressure of the Ahmed body car to study its dynamic behaviour. This fluid excitation was a time dependent loading which can be used to capture the transient modal dynamic response. A mixed mesh includes quadrilateral and triangular elements has been used to generate the surface mesh.
The mesh size range was set to be 10 mm to generate 20038 cells. Six sensors were located to capture the acceleration time history at particular locations.

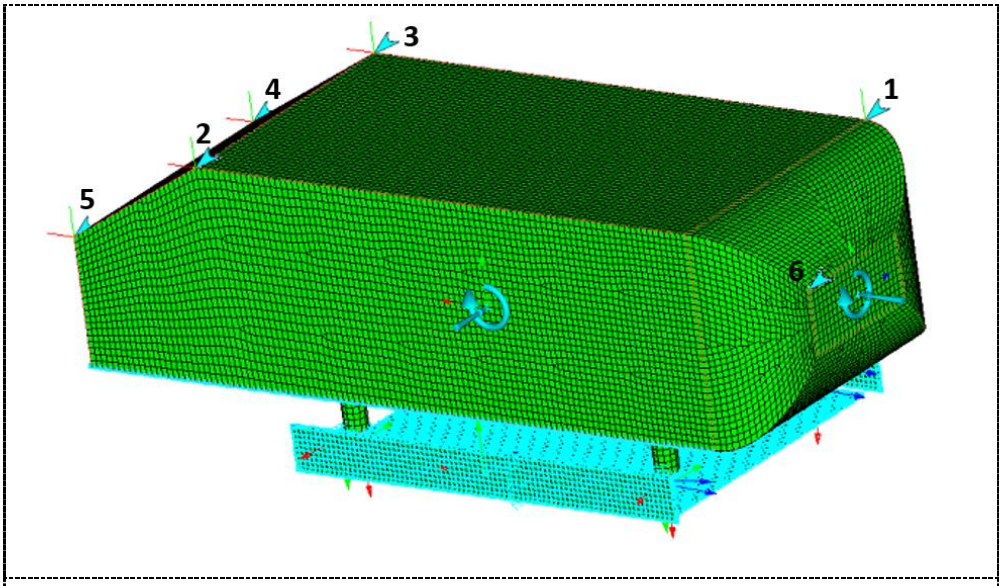

Figure 6. The location of dynamic loads and six sensors.

The simulation was accomplished in three stages, first, static pre-stiffening analysis, then, Modal extraction procedure and Dynamic analysis.
The eigen-frequency extraction procedure was conducted in order to extract the modes which includes the eigen-modes. This subset of modes is used to predict the structure's response. The analysis procedure is shown as follows:

- Processing the input data.
- Preparing Model topology data.
- Generating the model matrices.
- Assembling system matrices.
- Computing the normal modes and residual vectors has already being done in the modal analysis.
- Processing external loadings (the fluid excitation).
- Applying rigid-body constraints.
- Solving for unknowns.
- Generating model results.

8. Results and Discussion

8.1. CFD results

The aerodynamic coefficients have been obtained numerically and compared with the experimental data [25]. As shown in figure the numerical results are close to the experimental data with maximum

difference 5% between them. The focus will be on the aerodynamic effects on the overtaken car (stationary).

The side force is consistent with the experimental data between the positions from X/L=5 to X/L=1 without the influence of the overtaken car. However, between X/L=1 to X/L=0.5 the numerical side force is slightly larger than the experimental curve. The resultant fluid forces were obtained by multiplying the fluid pressure by the cross-sectional area of the body.

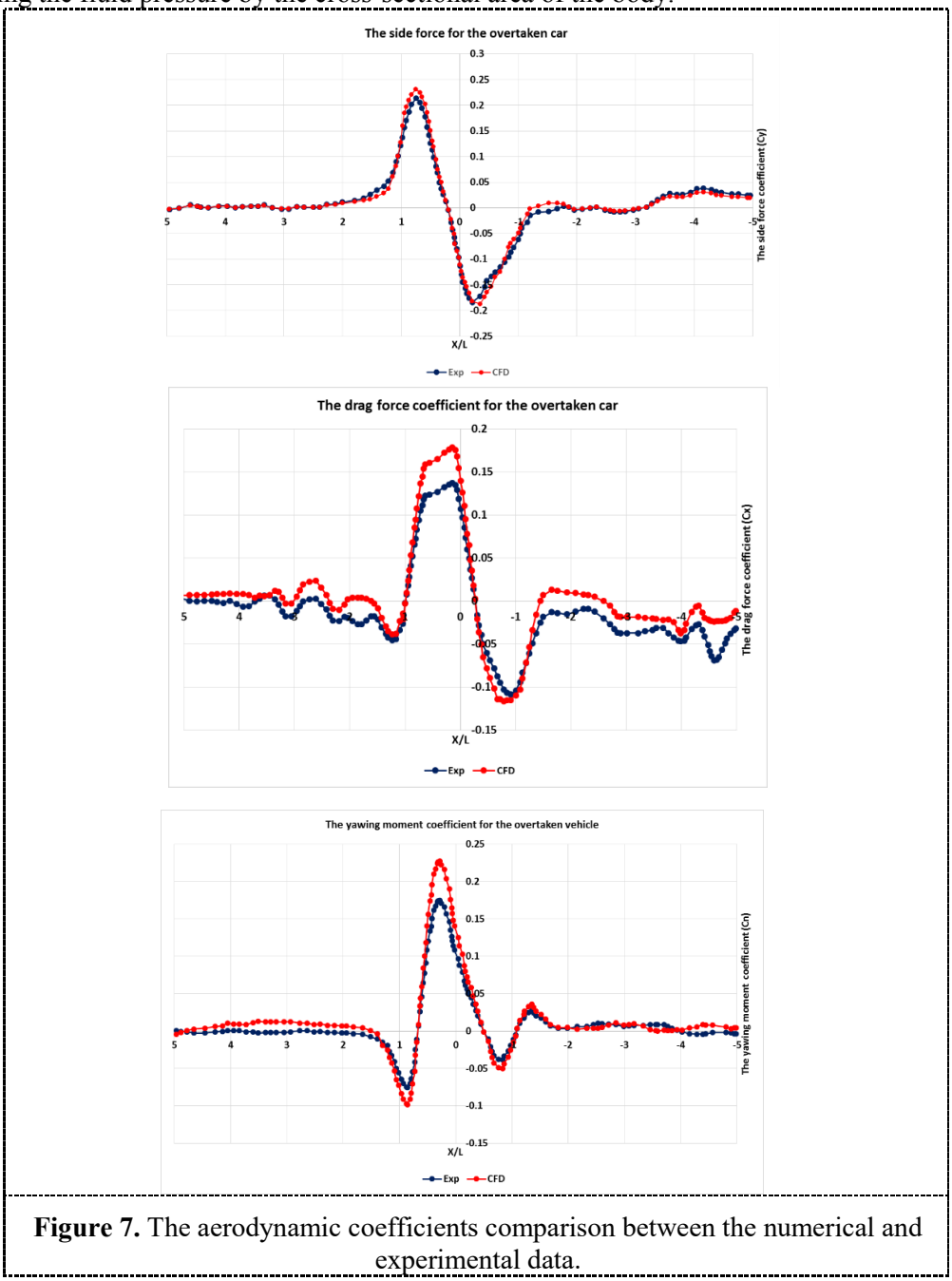

Figure 7. The aerodynamic coefficients comparison between the numerical and experimental data.

Figure (7) shows the aerodynamic coefficients acting on the overtaken (stationary) car1 during the computational analysis. The horizontal axis represents the dimensionless car location and the vertical axis represents the values of the aerodynamic force/moment coefficients. At the position between X/L=2 to X/L=1, it is clear that the drag is increasing when the overtaking event starts. This sudden impulse in the forces/moments is due to the high pressure in front of the moving car which leads to increase in pressure on the back panel of the stationary car. The pressure on the back panel of the stationary car will

then be reduced because of the negative pressure on the front panel of the moving car. This reduction will continue as the cars get closer and the flow will accelerate more. On the other hand, the side force increased because of the moving pressure which causes the pressure reduction on the back side of the stationary car. The yawing moment decreases as the pressure on the inner side of the stationary car is decreasing as well.

At the position between X/L=1 to X/L=0, the drag force keep increasing before it decreases due to the low pressure affects at the back of the stationary car reduces as the front edge of the moving car overtakes the back of the stationary car. The side force behaves slightly similar to the drag force as it increases then decreases because of the pressure reduction at the inner side of the stationary car. The back side of the stationary car will is pulled into the path of the moving car which will cause the yawing moment to increase. Then, the low pressure effect also on the front half of the stationary car which causes to nose to be pulled into the path of the moving car causing the yawing moment reduction.

At the position between X/L=0 to X/L=1, the front of the moving car will overtake the front of the stationary car, therefore, the low pressure in front of the moving car will certainly decrease the pressure at the region in front of the stationary car causing the drag force to decrease. Then, the back of the moving car will be alongside the front side of the stationary car and the overtaking manoeuvre is finished at this location which will return the drag force to the normal values. The side force increases as the low pressure on the inner side of the stationary car decreases which cause the two cars to repel each other. The yawing moment increases because of the flow separation behind the two cars and then decreases again. The decrease then come from the low pressure acting on the front half of the stationary car which will try to pull this half towards the path of the moving car. The surface pressure coefficient on the two cars is shown in figure (8) for a better understanding of the aerodynamic forces/moments explained above. Figure (8) shows also a comparison between the CFD data obtained from OpenFOAM and the CFD data published in [26]. A good agreement between the data can be shown clearly.

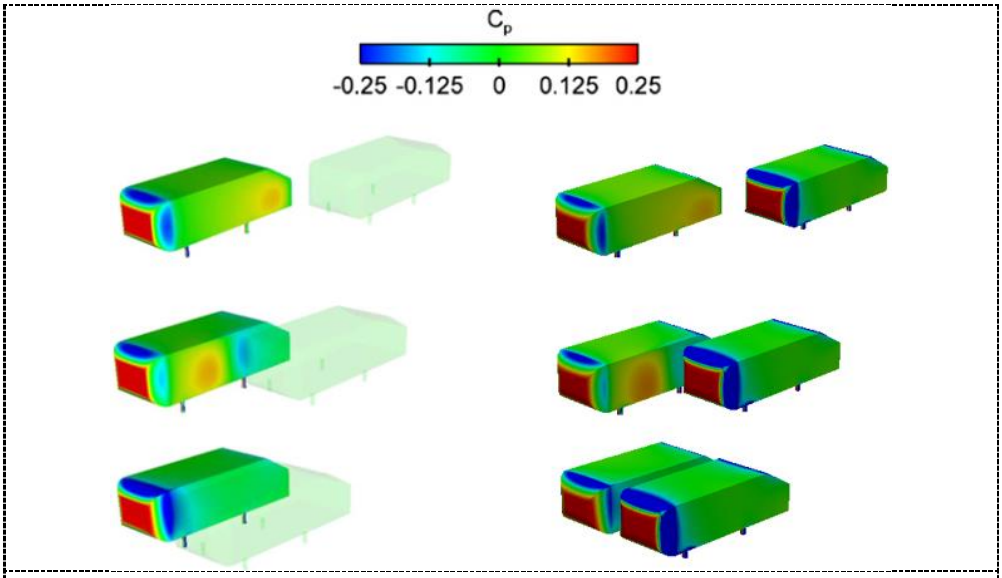

Figure 8. The comparison between two CFD data; CFD data from the open-source code used in this work (right); CFD published data (left)

The pressure coefficients were obtained by using the equation below:

$$C_P = \frac{P - P_\infty}{0.5\rho U^2} \tag{8}$$

Where: C_P denotes the pressure coefficient, $P - P_\infty$ is the relative pressure.

Note that the pressure coefficient is utilised in aerodynamic analysis to describe the pressure throughout the fluid field. It can be defined as a dimensionless number used to evaluate the airflow performance due to the presence of bluff bodies such as two moving cars inside the same tunnel. A complete aerodynamic analysis has been studied and performed to understand the effects acting on both cars. The above explanation showed that the OpenFOAM computational code is applicable to be trusted and its results are reliable. Figure (9) illustrates the all other aerodynamics effects which will be used to predict the dynamic response of the stationary car such as the lift force, the pitching and rolling moments.

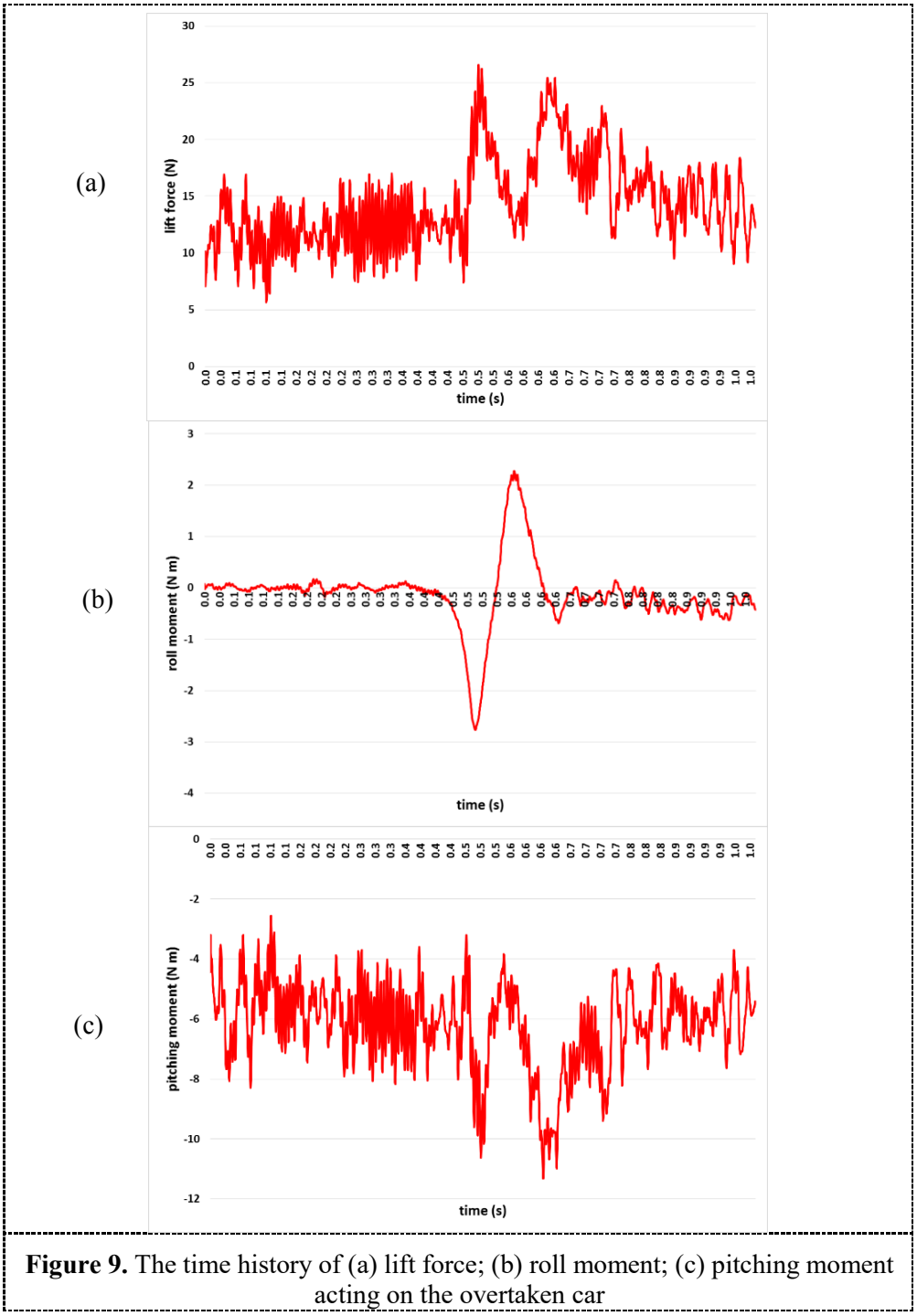

Figure 9. The time history of (a) lift force; (b) roll moment; (c) pitching moment acting on the overtaken car

8.2. FEA results

A finite element model was built by using a commercial software which is a powerful tool for simulating linear vibration analysis. The FEA software was also used for results visualisation. The stationary was modelled as a fully deformable body made of aluminium and the thickness is set to be 5mm.
Table 1 illustrates the natural modes of the Ahmed body oscillating system. The natural frequencies are calculated depending on the structure, material and boundary conditions.

Table 1. The natural modes and their natural frequencies

Mode	Natural frequency (Hz)
1	0.276
2	0.759
3	1.16
4	1.21
5	1.96
6	2.62
7	132
8	202
9	216
10	258
11	292
12	312
13	374
14	391
15	421
16	469
17	527
18	788
19	1100
20	1.5×10^6
21	2.64×10^6

The first six modes represent the rigid body modes and the modes from 7-21 represent the elastic body modes. In addition, the dynamic analysis have been accomplished by incremental method of frequency selection. The translational displacement response for the modes (3-6) can be shown in figures (10), (11), (12) and (13).

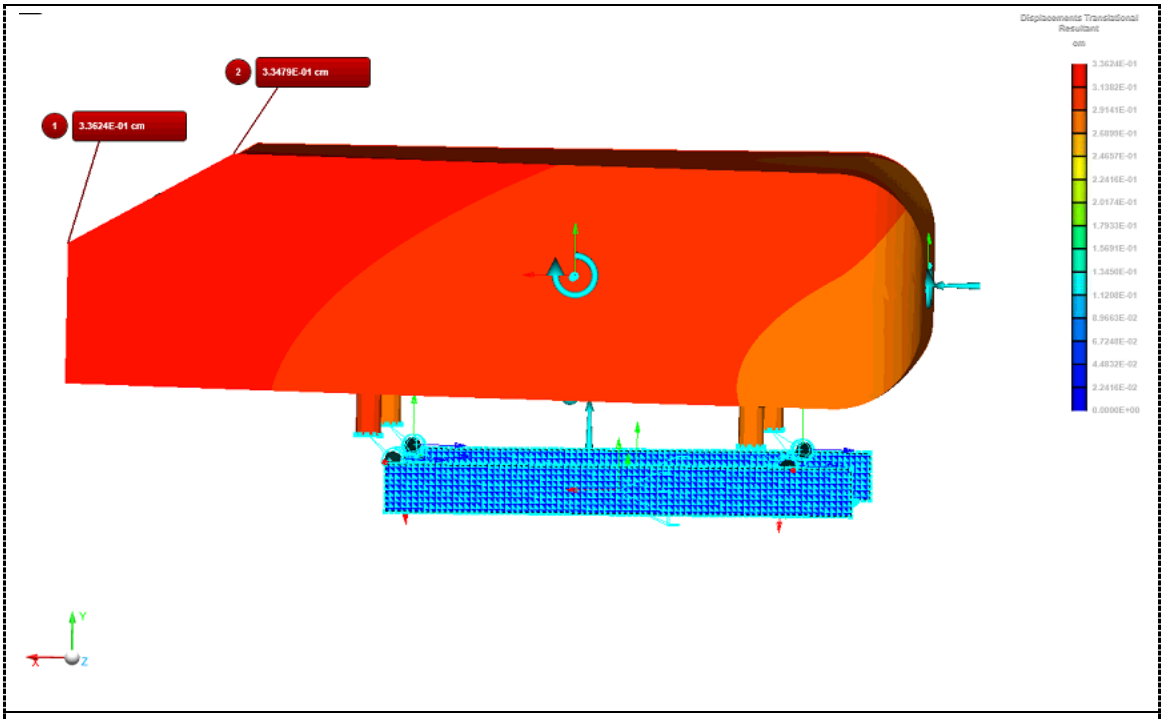

Figure 10. The fully dynamic response at the 3rd mode

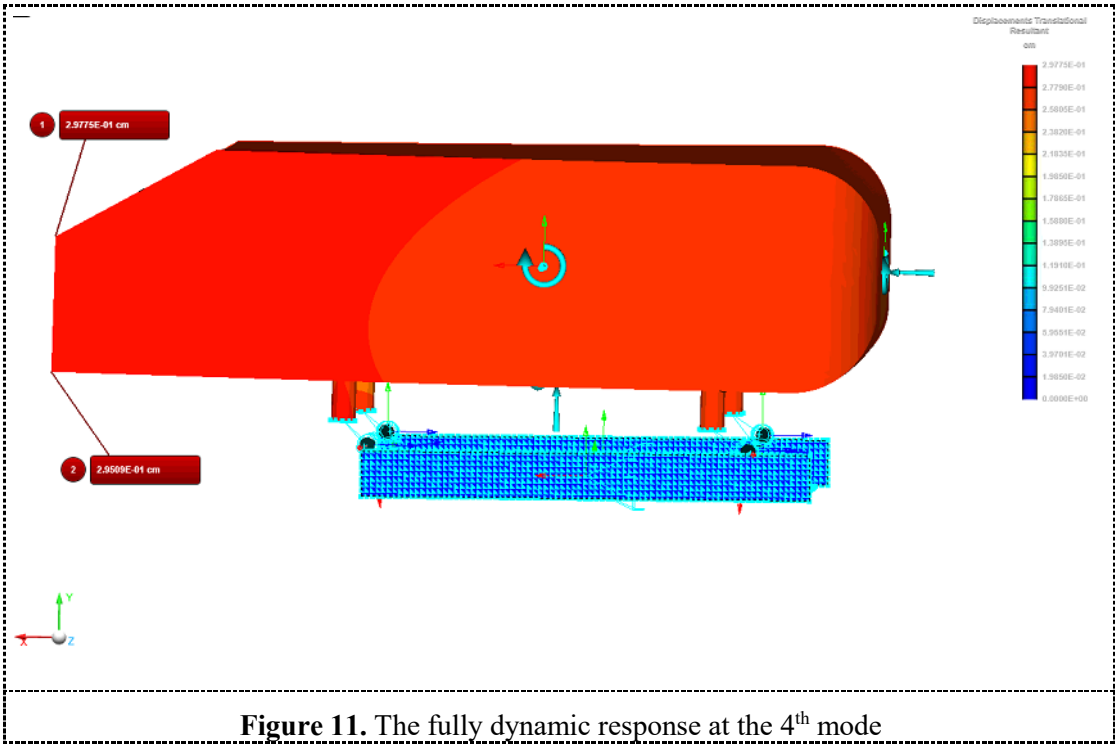

Figure 11. The fully dynamic response at the 4th mode

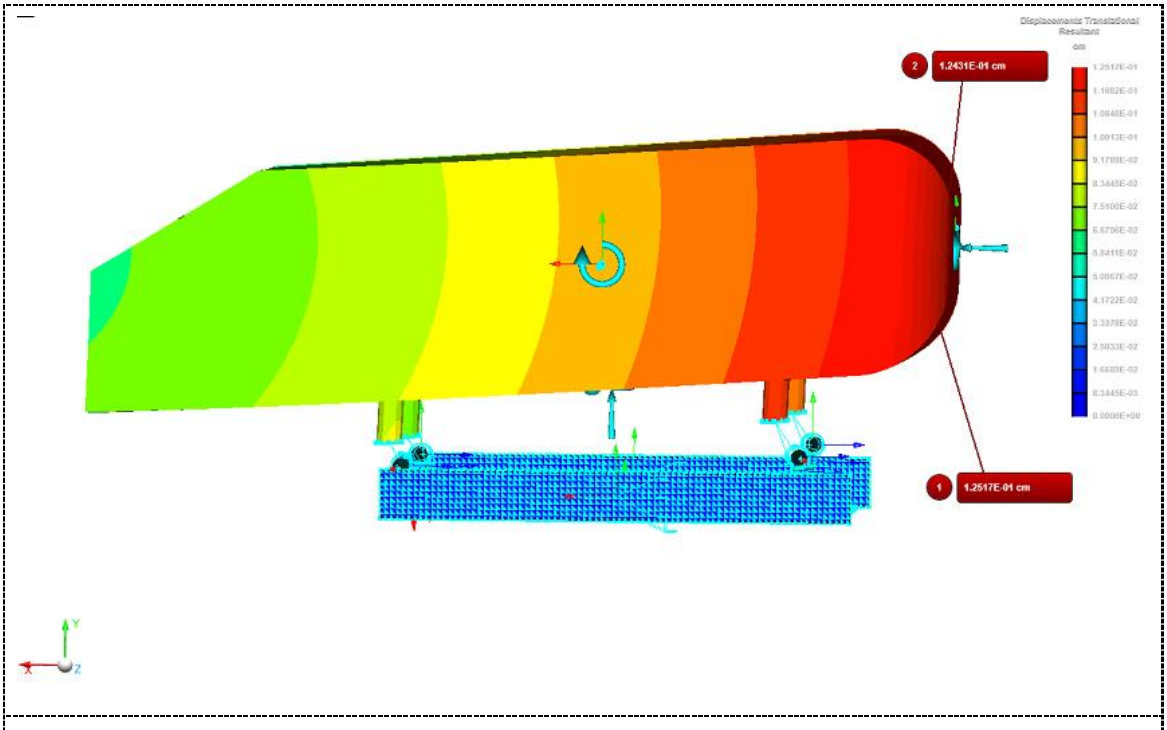

Figure 12. The fully dynamic response at the 5th mode

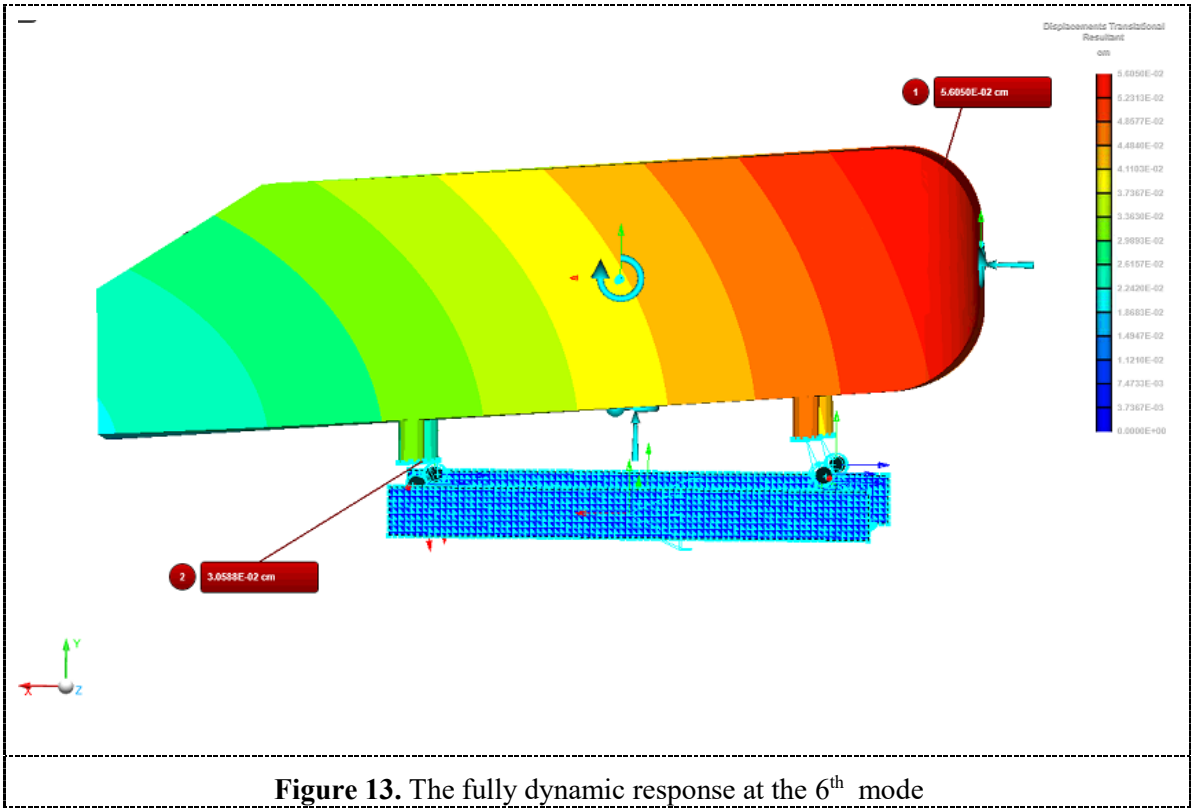

Figure 13. The fully dynamic response at the 6th mode

The maximum displacements for the rigid body frequencies are for 3rd, 4th, 5th and 6th are 0.34, 0.23, 0.19 and 0.056 centimetres, respectively.

Furthermore, the flexible body frequencies which cause the body deformation would be explained to identify the fluid forces contribution. As shown in figure (14), the top and bottom panels are influenced more by the dynamic lift force and the resultant translational displacement is equal to 7.9×10^{-5}cm.

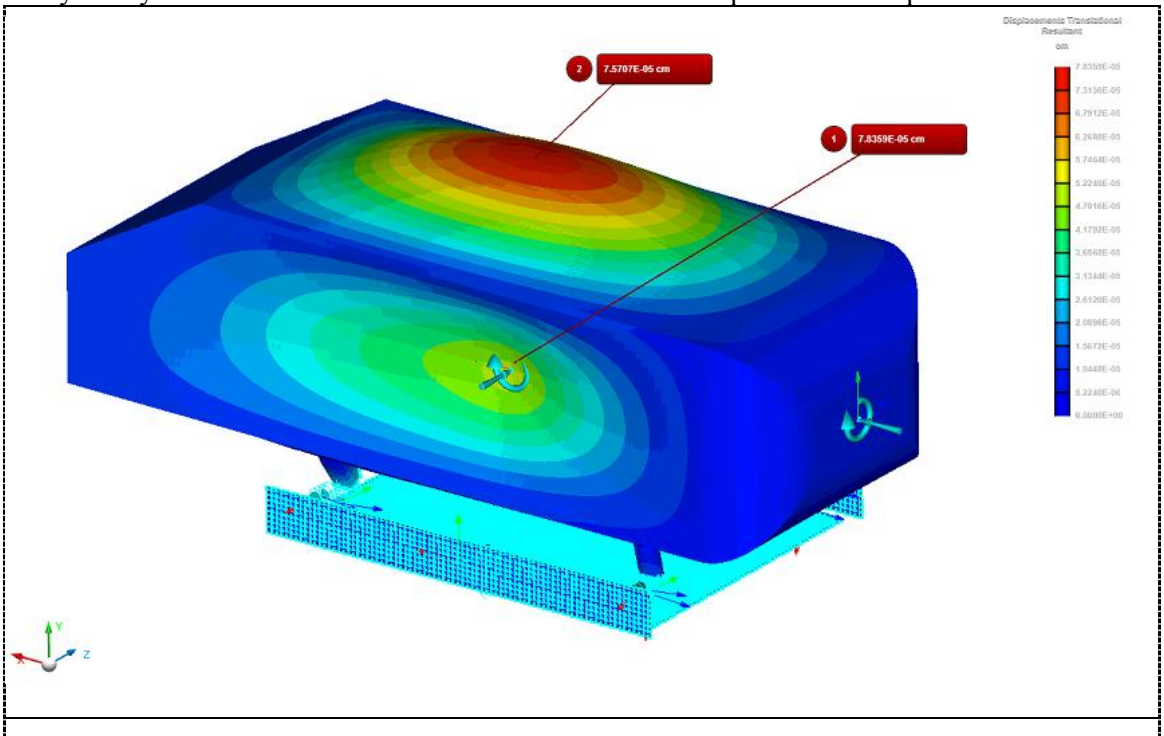

Figure 14. The fully dynamic response at the 7th mode

Nevertheless, the dynamic side force would be the main contributor in the 8th mode to deform the back half of the body bottom panel. The displacement is 1.2×10^{-4}cm as shown in figure (15).

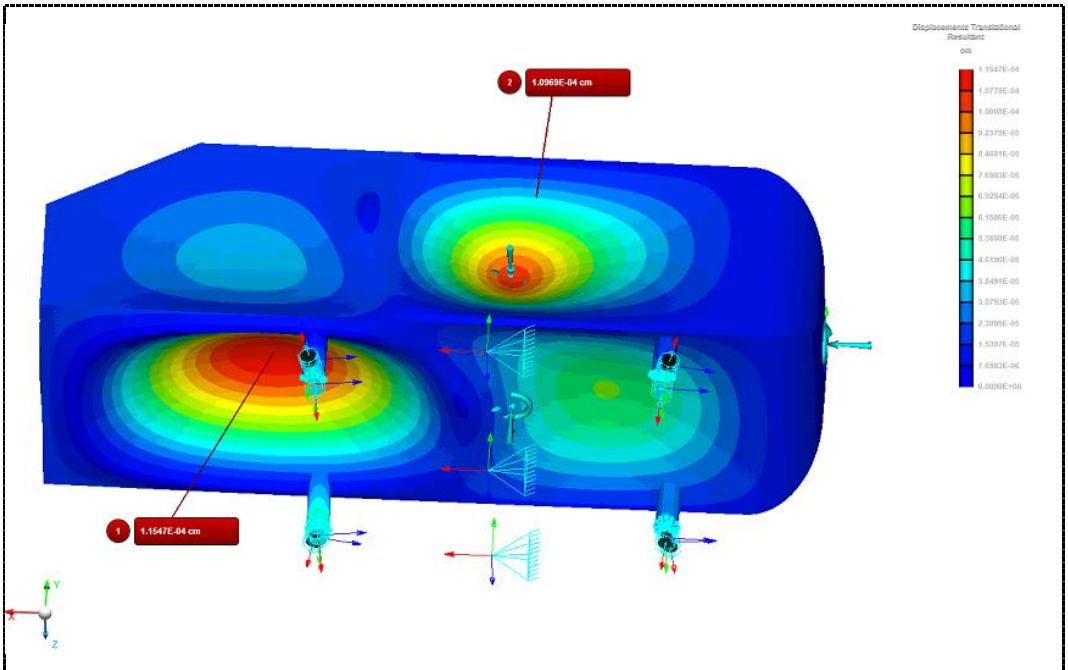

Figure 15. The fully dynamic response at the 8th mode

The frequency response has been calculated by the data conducted by the six sensors located on the body as shown in figure (6). The translational response shows the possible body oscillation as acceleration in a frequency domain. Figure (16) shows the body response to the lift force and yawing moment at the sensor (1) location. It is clear that the acceleration values increase at the natural frequencies. The maximum modal frequency is set to be at the 10th mode.

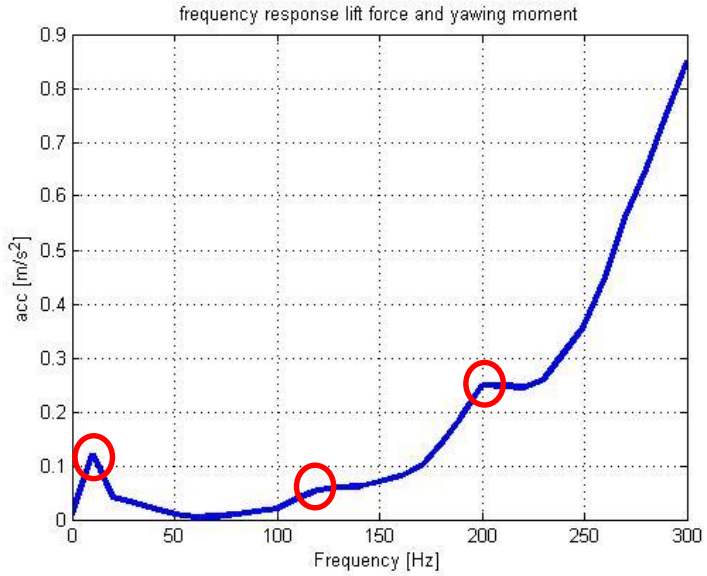

Figure 16. The frequency domain of the translational response of the body at sensor (1) cause by the lift force and yawing moment

The body response due to the dynamic side force and pitching moment is shown in figure (17). It shows also the magnitude spikes at the natural frequencies.

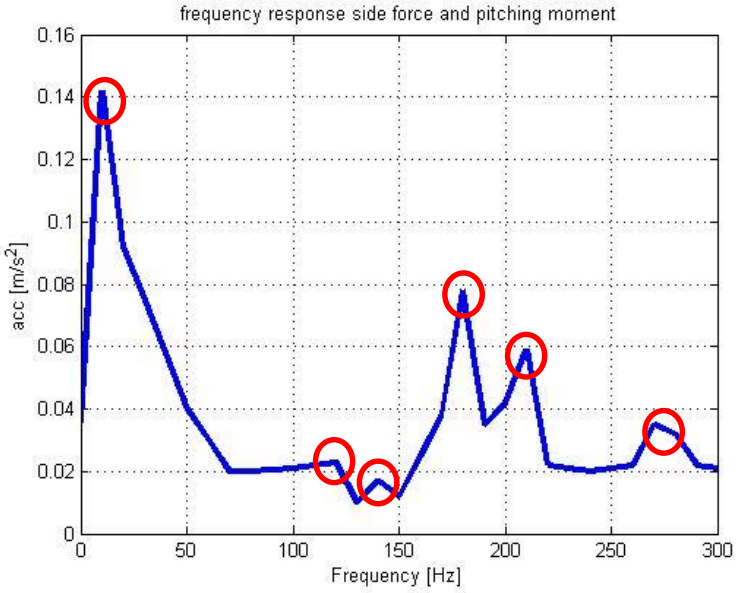

Figure 17. the frequency domain of the translational response of the body at sensor (1) cause by the side force and pitching moment

Interestingly, the drag force and rolling moment show a one high spike at the rigid body modes. While, the modes which cause deformation are not contributing as shown in figure (18).

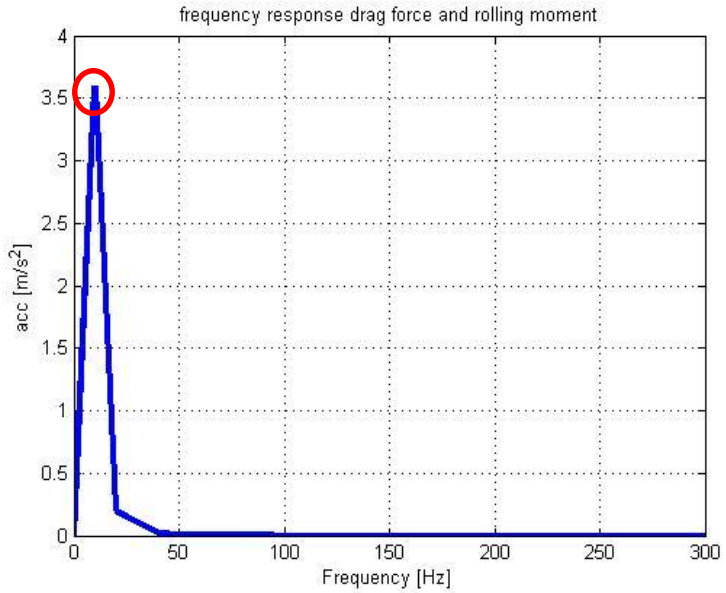

Figure 18. The frequency domain of the translational response of the body at sensor (1) cause by the drag force and rolling moment

By using the Inverse Fast Fourier Transformation (IFFT) operation [27], the frequency domain can be converted to time domain to show the body vibration as shown in figure (19).

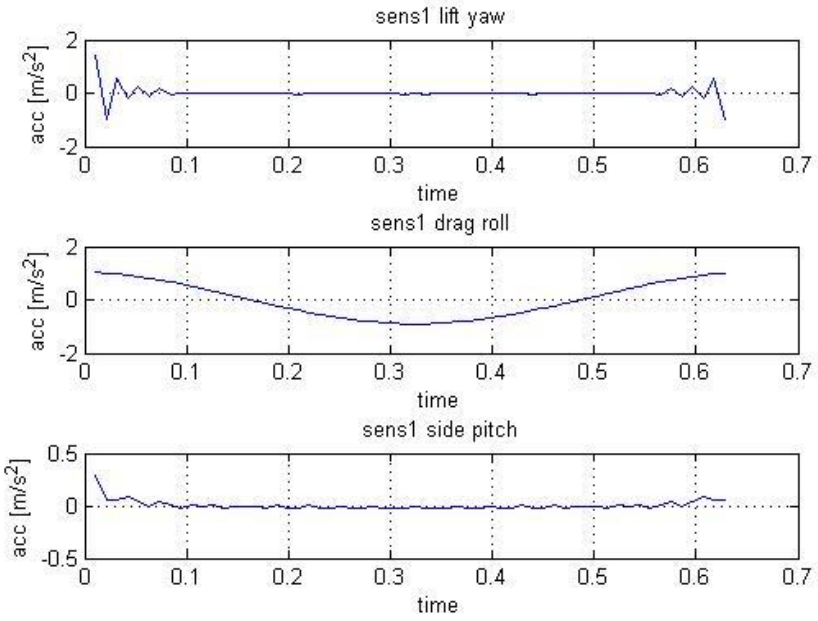

Figure 19. The time domain of the translational response of the body at sensor (1) location for the dynamic fluid excitations.

9. Conclusion

This paper examined the transient effects of fluid structure interaction of a freely vibrating Ahmed body during an overtaking manoeuvre. The Computational Fluid dynamics analysis has been achieved by the utilising an open-source package and some modifications to the code have been done. The dynamic fluid forces and moments have been constructed by running a steady and unsteady analysis.

Those aerodynamic loadings have been applied to the body as the only excitation to test their effect. A Finite Element Analysis has been accomplished by using a commercial software and the mode shapes, dynamic and frequency response have been studied. It is clear from this work that the fluid dynamics has a significant contribution to both the stationary and the moving cars. It was concluded that the transient phenomena is very important in terms of structural dynamics. This work has been done for only 1 second due to the computational cost, however, future work is required for longer CFD simulation in order to capture more data of aerodynamic effects. Overall, this study has proved that designers should consider the aerodynamic effects and make useful improvements to mitigate their effects.

References

[1] Zhang, B., Zhang, J., Yi, J., Zhang, N., Jin, Q. (2016) Modal and dynamic analysis of a vehicle with kinetic dynamic suspension system. Shock and Vibration. 2016.

[2] Sosnowski, M. (2018) The influence of computational domain discretization on CFD results concerning aerodynamics of a vehicle. Journal of Applied Mathematics and Computational Mechanics. 17(1), 79–88.

[3] Gallagher, M., Morden, J., Baker, C., Soper, D., Quinn, A., Hemida, H., Sterling, M. (2018) Trains in crosswinds – Comparison of full-scale on-train measurements, physical model tests and CFD calculations. Journal of Wind Engineering and Industrial Aerodynamics. 175, 428–444.

[4] Singh, N., Kaczmarczyk, S., Ehrl, T. (2017) An analysis of airflow effects in lift systems. In Lift and Escalator Symposium. The University of Northampton, CIBSE Lifts Group, LEIA, p. 24.

[5] Ahmed, S.R., Ramm, G., Faltin, G. (1984) Some Salient Features Of The Time-Averaged Ground Vehicle Wake.

[6] Huminic, A., Huminic, G. (2012) Numerical Flow Simulation for a Generic Vehicle Body on Wheels with Variable Underbody Diffuser.

[7] Ashton, N., Revell, A. (2015) Comparison of RANS and DES methods for the DrivAer automotive body. SAE Technical Paper.

[8] Tian, J., Zhang, Y., Zhu, H., Xiao, H. (2017) Aerodynamic drag reduction and flow control of Ahmed body with flaps. Advances in Mechanical Engineering. 9(7), 1687814017711390.

[9] Passalacqua, A., Laurent, F., Madadi-Kandjani, E., Heylmun, J.C., Fox, R.O. (2018) An open-source quadrature-based population balance solver for OpenFOAM. Chemical Engineering Science. 176, 306–318.

[10] Islam, H., Soares, C.G. (2018) Prediction of ship resistance in head waves using OpenFOAM.

[11] TotalSim Ltd. (2018) About TotalSim Experts in Computational Fluid Dynamics. [online]. Available from: https://www.totalsimulation.co.uk/about-us/ [Accessed March 14, 2018].

[12] IconCFD Ltd. (2018) ICON :: OpenFOAM®. [online]. Available from: http://www.iconcfd.com/services/consultancy/openfoam [Accessed March 14, 2018].

[13] OpenCFD Ltd (2018) Acquisition of OpenCFD Ltd., The leader in Open Source software in Computational Fluid Dynamics | ESI Group. [online]. Available from: https://www.esi-group.com/company/investors/news/acquisition-opencfd-ltd-leader-open-source-software-computational-fluid-dynamics [Accessed March 14, 2018].

[14] Solidworks, 2018. 3D CAD Design Software. Available at: https://www.solidworks.com/ [Accessed May 24, 2018].

[15] Apex, M. (2018) MSC Apex Modeler - Direct Modeling & Meshing Solution. [online]. Available from: http://www.mscsoftware.com/product/msc-apex-modeler [Accessed April 25, 2018].

[16] Noger, C., Regardin, C., Szechenyi, E. (2005) Investigation of the transient aerodynamic phenomena associated with passing manoeuvres. Journal of fluids and structures. 21(3), 231–241.
[17] Menter, F., Ferreira, J.C., Esch, T., Konno, B., Germany, A.C. (2003) The SST turbulence model with improved wall treatment for heat transfer predictions in gas turbines. In Proceedings of the international gas turbine congress. pp. 2–7.
[18] Ferziger, J.H., Peric, M. (2012) Computational methods for fluid dynamics. Springer Science & Business Media.
[19] Spalart, Pr., Allmaras, S. (1992) A one-equation turbulence model for aerodynamic flows. In 30th aerospace sciences meeting and exhibit. p. 439.
[20] Mohammad, A.F., Zaki, S.A., Ali, M.S.M., Yakub, F., Hagishima, A. (2018) Numerical Investigation of Wind-Induced Interference in a Random Urban Array.
[21] Friedrich-Karl Benra, Hans Josef Dohmen, Ji Pei, Sebastian Schuster, and Bo Wan, "A Comparison of One-Way and Two-Way Coupling Methods for Numerical Analysis of Fluid-Structure Interactions," Journal of Applied Mathematics, vol. 2011, Article ID 853560, 16 pages, 2011. https://doi.org/10.1155/2011/853560.
[22] WANG, F. and LI, S., (2018). Linearly Stable Periodic Solution for Lagrangian Equation. Journal of Computational Analysis and Applications, p.1454.
[23] Ariff, M., Salim, S.M., Cheah, S.C. (2009) Wall y+ approach for dealing with turbulent flow over a surface mounted cube: Part 2—High Reynolds number. In Proceedings of 7th International Conference on CFD in the Minerals and Process Industries CSIRO, Melbourne, Australia.
[24] KrajnoviÄ, S., Bengtsson, A., Basara, B. (2011) Large eddy simulation investigation of the hysteresis effects in the flow around an oscillating ground vehicle. Journal of Fluids Engineering. 133(12), 121103.
[25] Noger, C., Széchényi, E. (2004) Experimental study of the transient aerodynamic phenomena generated by vehicle overtaking. Flow Induced Vibration.
[26] Uystepruyst, D., Krajnović, S. (2013) Numerical simulation of the transient aerodynamic phenomena induced by passing manoeuvres. Journal of Wind Engineering and Industrial Aerodynamics. 114, 62–71.
[27] Ida, Y., Matsumoto, T., Matsufuji, S. (2018) Packet splitting and adaptive modulation based on CSI of time domain for decode-and-forward cooperative OFDM systems in different channel model. International Journal of Communication Systems. 31(2).